

Article

Evaluation of Vibration Detection Using Smartphones in a Two-Story Masonry-Infilled RC Frame Building

Jae-Do Kang ^{1,*}, Eun-Rim Baek ²  and Sung-Ho Park ¹¹ Division of Urban Infrastructure Research, Seoul Institute of Technology, Seoul 03909, Republic of Korea² Seismic Research and Test Center, Pusan National University, Busan 50612, Republic of Korea

* Correspondence: kang@sit.re.kr

Abstract: For measuring the structural health of buildings, high-performance vibration detection devices are used in a structural health monitoring (SHM) system, which consists of a sensor and a data logger. Those devices are seismographs or devices with high-performance sensors which are expensive. Recently, smartphones are being used as seismographs to accumulate big data of earthquake wave detection because they have accelerometers of microelectromechanical systems. Since a smartphone has the functions of a detection sensor and a data logger, a low-cost SHM system can be developed by using a low-cost smartphone. In this paper, smartphones were used to confirm the possibility of the development of a low-cost SHM system. To evaluate the vibration detection performance from small displacement and large displacement, smartphones were installed in a specimen of a large shaking table test. The specimen is a scale model of a two-story non-reinforced masonry-filled reinforce concrete (RC) frame building. The natural period and interstory drift ratio were used as the evaluation criteria. The natural period estimated by the smartphone data agreed with that found by the piezoelectric accelerometer data. For estimating the building deformation, which is related to building stability, the measurement performance for large deformation using smartphones was evaluated. The smartphones have 90% or higher accuracies for the estimation of the maximum acceleration and displacement.

Keywords: iOS smartphones; i-Jishin; acceleration detection; structural health monitoring; MEMS sensor



Citation: Kang, J.-D.; Baek, E.-R.; Park, S.-H. Evaluation of Vibration Detection Using Smartphones in a Two-Story Masonry-Infilled RC Frame Building. *Buildings* **2023**, *13*, 1069. <https://doi.org/10.3390/buildings13041069>

Academic Editors: Serena Cattari, Ilaria Venanzi and Philippe Gueguen

Received: 13 March 2023

Revised: 3 April 2023

Accepted: 16 April 2023

Published: 18 April 2023



Copyright: © 2023 by the authors. Licensee MDPI, Basel, Switzerland. This article is an open access article distributed under the terms and conditions of the Creative Commons Attribution (CC BY) license (<https://creativecommons.org/licenses/by/4.0/>).

1. Introduction

In Japan, with the aim of detecting strong vibrations due to earthquakes, strong-motion accelerographs, termed Strong Motion Acceleration Committee (SMAC) accelerographs, were developed after the 1948 Fukui earthquake. SMAC accelerographs found application in the detection of building vibrations in Japan in the 1950s. The Japan Building Research Institute (BRI) installed SMAC accelerographs in approximately ten buildings [1,2]. In Niigata City, SMAC accelerographs recorded the collapse of a building caused by soil liquefaction during the 1964 Niigata earthquake [2,3]. In 1973, the National Strong Motion Project (NSMP) in the U.S. was absorbed by the U.S. Geological Survey as part of the National Earthquake Hazards Reduction Program for acquiring strong motion records [4]. At this time, the idea was to monitor building vibrations for recordings of damaging earthquakes, which are critical for designing earthquake-resistant structures. The data recorded in the U.S. and Japan were used for evaluations of structural response and correlated performance [5]. In Europe, the earthquake detection network systems have operated to record and analyze earthquake waveforms and to provide high-quality data, for example, ref. [6,7]. Richardson [8] developed technology for damage detection in structures caused by changes in their dynamic (modal) properties. This study focused on structural integrity monitoring for large structures. With the development of devices and technologies, in 1996, Doebling et al. [9] provided a comprehensive review of the technical literature on the detection, location, and characterization of structural damage. The damage caused by

fatigue and external loads (e.g., earthquakes and winds), may progress very slowly [10]. The damage becomes observable only when the structural damage is considerable. Using changes in the measured structural vibration response, the techniques examined in this report [9] estimated the structural damage. This is similar to structural health monitoring (SHM), which aims to estimate the behavior and performance of structures during their life cycle and predict their remaining service life. In SHM, the knowledge and experience in civil, mechanical, electrical, computer, and control engineering are used in assessing the health of structures [11]. In the past three decades, many researchers have worked on SHM [12–16]. Based on the acting load, there are two kinds of SHM methods, static and vibration based [11,17,18]. By measuring the static responses of structures such as strain [19,20] and deflection [21], static-based damage detection methods estimate the health of structures. Vibration-based damage detection methods primarily assess the modal parameters of a structure using system identification methods [22]. In applications using vibration-based damage detection methods, the estimation accuracy depends on the performance of the vibration measurement sensors, the improvement of which requires knowledge and experience in mechanical, electrical, and computer engineering. For detection of earthquake events, some countries have operated seismic stations, for example, [23–26]. Seismographs, which are used as one of the devices at seismic stations, can conduct high-performance vibration measurements. Therefore, seismographs or devices with improved technology [27,28], such as P-wave alert devices (P-Alert) and IT strong-motion accelerographs, are used to detect structural vibrations. P-Alert was developed by a research group at the National Taiwan University for use in earthquake early warning (EEW) systems. P-Alert uses accelerometers of microelectromechanical systems (MEMS). MEMS accelerometers have been tested and applied in detecting vibrations of infrastructure, buildings, and the ground [29–35]. They are also installed in smartphones. Therefore, smartphones have been investigated as a substitute for seismometers [36,37]. The “MyShake” app was developed as an EEW system and uses a classifier algorithm to identify earthquake vibrations on a single phone [36]. Further, the “i-Jishin” app was developed for measuring earthquakes by the National Research Institute for Earth Science and Disaster Resilience of Japan; it makes use of MEMS acceleration sensors incorporated in the mobile information terminals. The measurement settings of the “i-Jishin” app can be modified in terms of the sampling rate, leading allowance time, following allowance time, and trigger to record, and can calculate the velocity and displacement from acceleration [37]. Since a smartphone has the functions of a detection sensor and a data logger, a low-cost SHM system can be developed when using a low-cost smartphone. For developing the low-cost SHM system, the measurement settings of another app, the “accmeasure” app, can also be modified in terms of the sampling rate, leading allowance time, following allowance time, and trigger to record [38]. The two aforementioned apps may be used in SHM because they feature functionalities such as trigger to record and a sampling rate of 100 Hz, setting record time, and time synchronization; their use has been investigated for SHM [38,39]. To estimate the structural health, some researchers used smartphones [40–45]. These can almost estimate the detection performance of the small accretion of small displacement. In architectural engineering, large deformation, such as interstory drift, should be detected. However, the “i-Jishin” app was not evaluated for the estimation of interstory drift. Therefore, the measurement performance of the smartphone for large deformation of a structure close to the full scale should be evaluated.

Given the above, the objective of this study is to evaluate the vibration detection performance of a smartphone with the “i-Jishin” app installed in estimating the large deformation of a building. In addition, the prediction performance of dynamic characteristics, such as the natural period, was also estimated. Those are achieved by comparing the data measured by a reference accelerometer, which is a piezoelectric accelerometer from the PCB Piezotronics Company, wire displacement sensors and a smartphone-installed specimen in shaking table experiments. The specimen is a two-story masonry-infilled RC frame building, which is the standard design of low-story school buildings or residential buildings in

Korea. For estimating large deformation of a building, the displacement calculated from the acceleration measured by the smartphone was compared with displacement of the building measured by the experiment. Additionally, the natural periods estimated by the transfer function of acceleration measured by the reference accelerometer and smartphone were compared.

2. Materials and Methods

2.1. Specimen Design

The purpose of the shaking table test is to evaluate the seismic performance of existing buildings. To this end, a masonry-filled RC frame building, which is the standard design of school buildings and other commercial or residential buildings, was selected as a target. In this study, a specimen was designed based on a standard drawing of low-story school buildings or residential buildings in Korea. The specimen, which was an approximately 60% scale model of a school building, was a two-story non-reinforced masonry-filled RC frame building (Figure 1 and Table 1). Figure 1a shows the setup of the shake table test. As shown in Figure 1b, openings were installed at the front and rear of the specimen considering the actual building geometry. The specimen had a 3000 mm × 3000 mm square plane with a floor height of 1830 mm and a total height of 3780 mm (Figure 1c,d). The masonry infill wall on each floor had a length (L) of 2600 mm, height (H) of 1530 mm, an aspect ratio (H/L) of 0.59, and masonry wall thickness of 60 mm. Considering that the specimen was a scale model, the bricks were stacked in an upward direction; nevertheless, the thickness of the masonry infill wall was 57 mm. The concrete used for the frame of the specimen had a nominal compressive strength of 18 MPa, and SD400 (steel deformed bar with yield strength of 400 MPa) was used as a steel reinforcement. The size of the column was 200 × 200 mm. Four D13 (diameter of 13 mm) reinforcing bars were used as the main reinforcement, and the hoop used was a closed hoop with D6 (diameter of 6 mm) at 120 mm spacings. The size of the beam was 200 × 300 mm. Four D13 reinforcing bars were used as the main reinforcement, with two placed in the upper part and two in the lower part. The stirrup was a closed stirrup that used D6 at 120 mm spacings. The thickness of the slab was 120 mm, and D10 (diameter of 10 mm) was placed at 120 mm spacings as horizontal and vertical reinforcements. The first floor formed the shape of a T-beam, whereas the second floor used bolts to connect the slab and beams and facilitate the connection of load blocks on the second floor and roof. In addition, a weight of 96 kN was installed at the upper parts of the first and second floors, respectively, considering the axial load of the column and the upper load.

Table 1. Design of specimen.

Item	Target Building	Specimen	Scaling Factor
Dimension (Depth × Width × Height), (unit: mm)	7000 × 9000 × 3600	2800 × 3600 × 1800	0.6 (Height 0.5)
Story	3	2	-
Column (unit: mm)	350 × 400 or 350 × 500	200 × 200	0.5~0.57
Beam (unit: mm)	300 × 600 or 300 × 450	200 × 300	0.33
Shear force in longer direction	240 kN	37 kN	0.15
Shear force in shorter direction	161 kN	37 kN	0.23
Column axial force ratio	0.13	0.17	
Masonry wall thickness	0.19 (1.0B)	0.06	0.32

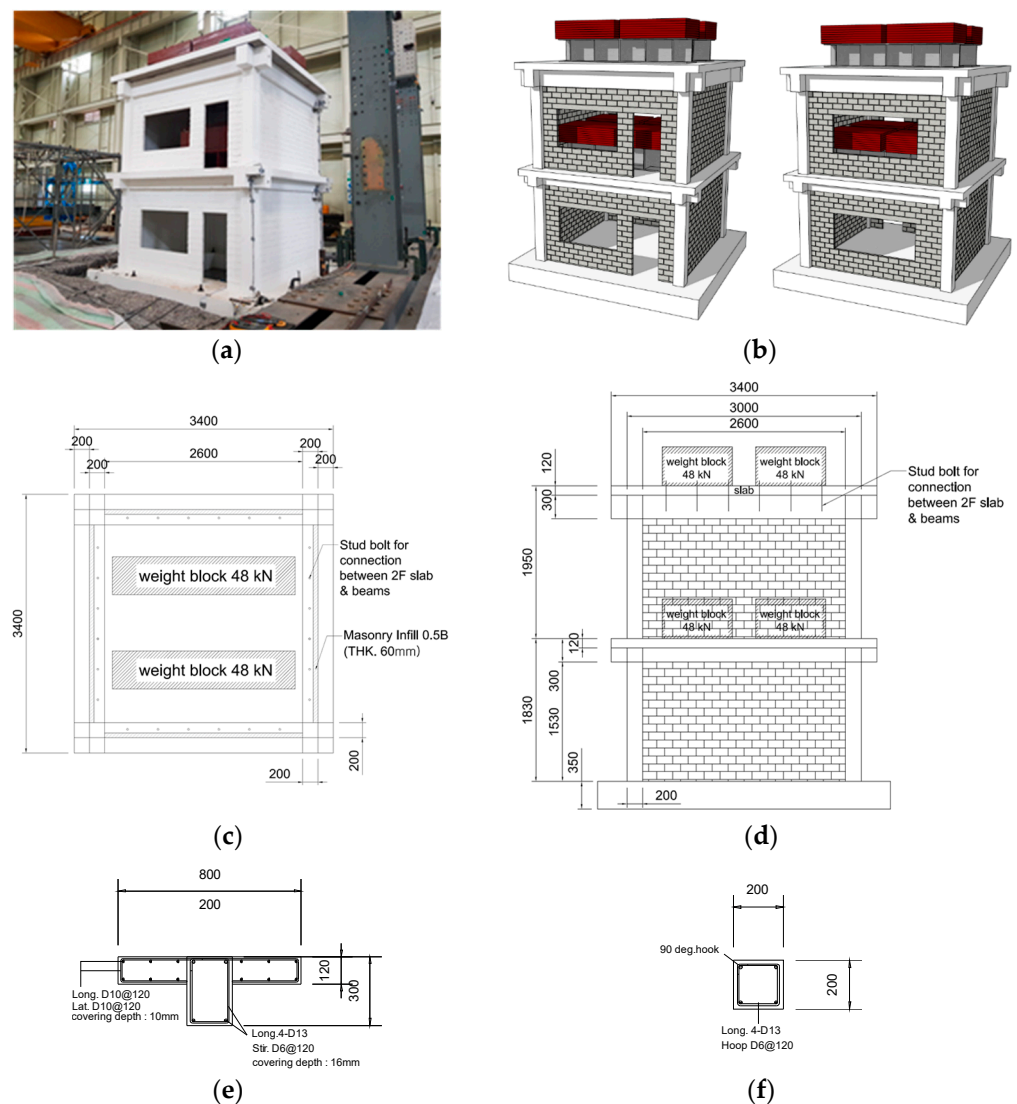


Figure 1. Configuration of specimen (unit: mm): (a) photo; (b) aerial view from the front (left) and the rear (right); (c) plan; (d) elevation; (e) beam and slab; (f) column.

2.2. Shaking Table Test

The shaking table used in this study had three degrees of freedom and was installed in the Yangsan campus of Pusan National University. The size and specifications of the shaking table are shown in Table 2.

Table 2. Performance of shaking tables.

Item	Performance
Max. loading (kg)	60,000
Table size (mm)	5000 × 5000
Control axes	3 DOF (2 translational axes, 1 rotational axis)
Max. displacement (mm)	X-Axis = ±300, Y-Axis = ±200
Max. velocity (m/s)	Hor. (X, Y) = 1.0
Max. acceleration (g)	Hor. (X, Y) = ±3.0 (at bare table)
Frequency range (Hz)	(0.1–60.0)
Excitation mechanism	Electro-hydraulic Servo, 3-variable control
Control software	MTS 469D
Feedback data acquisition	51 channels (Sampling rate = 512 Hz)

In the resonance frequency search test to evaluate the natural period, which is the dynamic characteristic of a specimen, excitation was performed using white noise vibration waveforms in the forward/backward (Y) and left/right (X) directions. The zero-period acceleration (ZPA) of the excitation wave was set to an RMS average of 0.05 g, and the input frequency was set to range from 0.5 to 50.0 Hz, considering the characteristics of the shaking table and input waveform. The excitation duration was 30 s.

For the earthquake waveform in the shaking table test, an artificial earthquake wave that meets the designed seismic load of South Korea was generated and applied. The design acceleration spectrum used in the test was one that corresponds to seismic zone 1, S3 soil, and a short-period design spectral acceleration (SDS) of 0.54 g, which are suggested in the KDS 41 17 00 building seismic design standards (Figure 2a). For the input seismic wave, an artificial earthquake wave corresponding to a magnitude 7 earthquake, which meets the design acceleration spectrum, was created (Figure 2b). The acceleration and time interval were adjusted according to the similarity law (Table 1) considering that the specimen was a scaled model. The artificial seismic wave was applied after adjusting its scale to 30, 60, 100, and 150%. The detailed procedure of excitation is shown in Table 3.

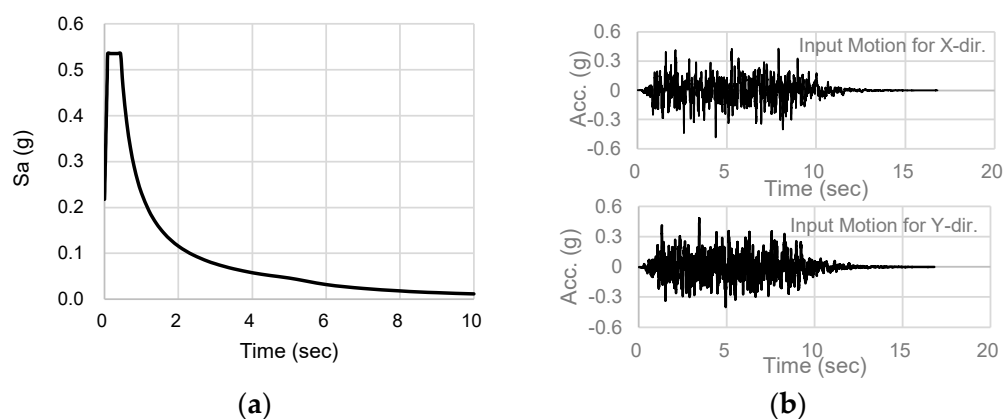


Figure 2. Artificial accelerograms: (a) design spectrum; (b) waveform.

Table 3. Test procedure and smartphone measurement.

Test No.	Excitation	Direction	Scale (%)	Peak acc. (g)	Smartphone Error		
					First Floor	Second Floor	Roof Floor
1	Random, 30 s	X	100	RMS 0.05	-	-	-
2	Random, 30 s	Y	100	RMS 0.05	-	-	-
3	Artificial accelerograms	XY	30	0.14	-	-	-
4	Artificial accelerograms	XY	60	0.29	-	Error	Error
5	Artificial accelerograms	XY	100	0.48	-	Error	Error
6	Artificial accelerograms	XY	150	0.72	-	Error	Error

2.3. Measurement System

To measure the seismic responses of the main parts of the specimen, accelerometers, displacement sensors, and strain gauges were installed at the main positions. A total of six accelerometers were installed at the main positions, including the floor of the shaking table, the base of the second floor, and the base of the roof floor, to measure the acceleration in the forward/backward and left/right directions on each floor. In addition, wire displacement sensors were installed at eight positions on the left and right sides of the first and second floor beams, on the right side and rear of the specimen, to measure the story drift in each direction. Eight displacement sensors were additionally installed in the upper right corner of the masonry infill walls, with no opening on the left and right sides of the specimen, to measure the gap between the frame and masonry infill wall in the horizontal

and vertical directions on each floor. Strain gauges were attached to the lower and upper parts of the first-floor column, the lower part of the second-floor column, and the left/right main reinforcement and stirrups of the first-floor beam before pouring concrete. Figure 3a shows the positions of the accelerometers and displacement sensors used in this study. Data were recorded at 512 Hz. The measured acceleration and displacement data, however, were resampled to 100 Hz for comparison with the smartphone data.

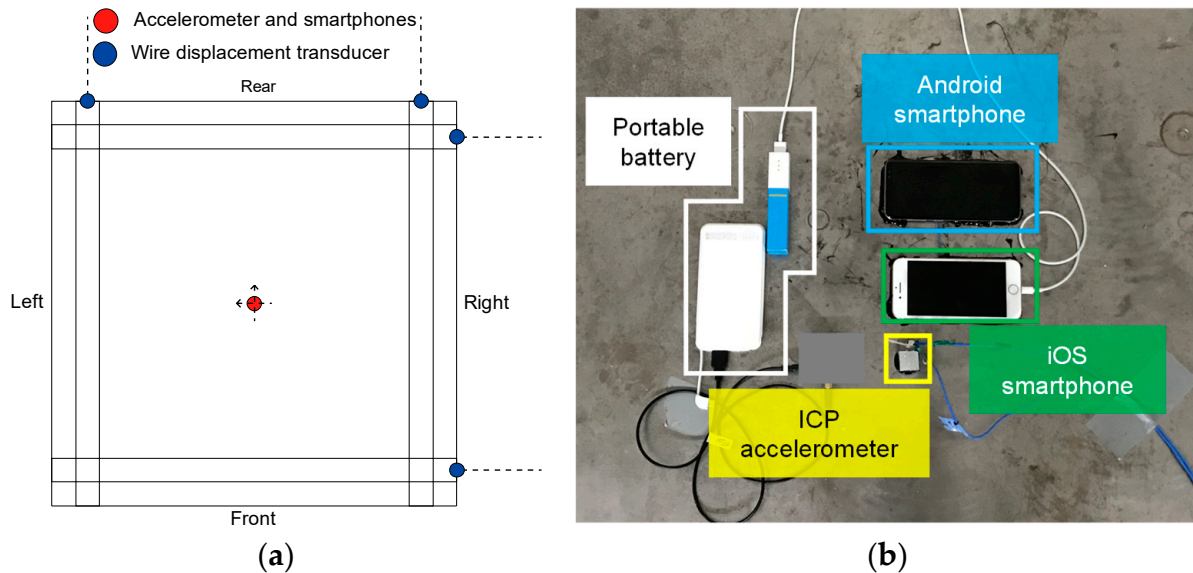


Figure 3. Installation of sensors: (a) sensor position; (b) smartphones.

2.4. Smartphone Measurement

In an additional test, smartphones were installed at the center of the floor on each floor to evaluate their vibration measurement accuracy, and portable batteries were connected to them to prevent them from being turned off during the test (Figure 3b). Three iOS smartphones and three Android smartphones were used in the test. For vibration measurements, the “i-Jishin” app developed by the National Research Institute for Earth Science and Disaster Resilience in Japan [37] was installed in the iOS smartphones. On the other hand, in the Android smartphones, the vibration measurement test application developed by the research team of this study was installed. For the purpose of this study, only the results obtained using the iOS smartphones (iPhone 7, 8, and X) were used. A trigger was set such that vibrations over 10 cm/s^2 could be recorded when measured. In addition, the vibration measurement application was running at all times. The sampling rate of the application was set to 100 Hz. Since each smartphone performed measurements independently, all were connected to Wi-Fi for time synchronization with the NTP server. Although the i-Jishin application was equipped with the FFT transmission function, this function could not be used in this study due to the network environment.

3. Results and Discussion

3.1. Application Measurement Characteristics

After the vibration test, the data measured by the i-Jishin application used in this study were analyzed. Table 3 shows that there is no measurement error in the data from the smartphone installed on the first floor. However, in the smartphone installed on the roof, the acceleration was not recorded in tests 4 to 6. This is because the smartphone used in these experiments had low battery capacity and the connected portable battery could not fully charge the phone due to its low capacity. This issue needs to be addressed in future tests. In the smartphone installed on the second floor, the acceleration was recorded in tests 4 to 6, but the data could not be used due to errors. It was found that the errors occurred as the brick separated from the wall, which impacted the smartphone during test 4. In future

tests, measures to prevent damage to smartphones are required. Although the smartphones were connected to Wi-Fi installed in the experimental building for time synchronization with the NTP server, synchronization could not be performed well due to the influence of the experimental building environment. Time synchronization was performed using the MATLAB algorithm (finddelay function) to analyze the measurement characteristics. This MATLAB algorithm estimates the normalized cross-correlation between two signals and estimates the lag based on the lag value for which the normalized cross-correlation has the highest absolute value [46]. In evaluating the vibration detection performance using data obtained from the white noise excitation tests, a 0.2–25 Hz band filter was applied to the acceleration measured with the reference accelerometers and smartphones.

3.2. Natural Period Evaluation

The natural period was estimated by calculating the transfer function of the acceleration measured at the center of each floor in the specimen and using the curve fitting technique. In this study, five Lorentzian curves (red dotted lines in Figure 4) having a high agreement with the transfer function (black solid lines in Figure 4) between 0 and 10 Hz were extracted. After then, the natural period (blue dotted lines in Figure 4) was estimated from the curve with the maximum value. Analysis of the data obtained from the reference accelerometer revealed that the natural period was 0.25 s in the X direction and 0.14 s in the Y direction (Figure 4). The natural period estimated with the smartphone measurements was identical to that estimated with the reference accelerometers (Figure 4). This implies that the natural period of a building can be evaluated using smartphones if vibration occurs with the same magnitude as in the white noise excitation test.

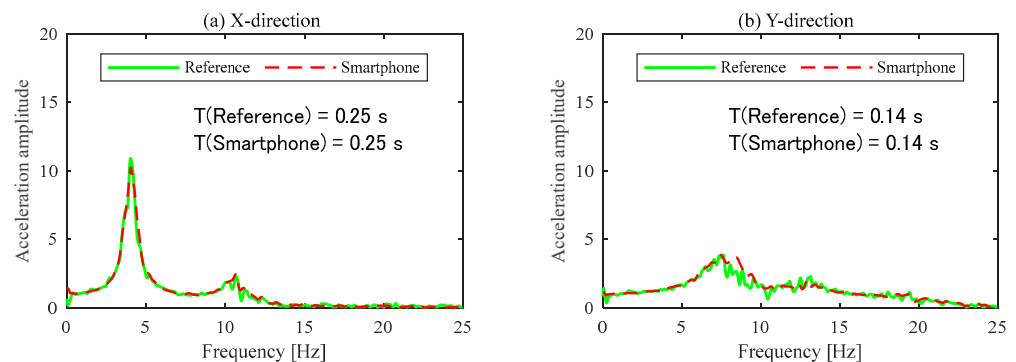


Figure 4. Estimated natural period.

3.3. Acceleration Measurement Accuracy

To quantitatively evaluate the error of the acceleration waveform measured by the smartphones, the root-mean-square percentage error (RMSPE) values between the measurements obtained with the reference accelerometers and smartphone in the time domain were evaluated using the magnitude-squared coherence function (MSCF) values of the same measurements in the frequency domain. The RMSPE was calculated as follows:

$$\text{RMSPE} = \sqrt{\frac{1}{n} \sum_{k=1}^n \left(\frac{x_{\text{smartphone}} - x_{\text{icp}}}{x_{\text{icp}}} \right)^2}, \quad (1)$$

where x_{icp} is the measured acceleration using the reference accelerometers and $x_{\text{smartphone}}$ is that using smartphones. For a and b signals, the MSCF [47,48] is defined as follows:

$$C_{ab} = \gamma_{ab}^2(f) = \frac{|G_{ab}(f)|^2}{G_{ab}(f)G_{ab}(f)}, \quad (2)$$

where $G_{aa}(f)$ and $G_{bb}(f)$ denote the power spectral density of a and b signals and $G_{ab}(f)$ denotes the cross spectral density of a and b signals. The MSCF is a function of the frequency, with values between 0 and 1. These values indicate how well the two signals correspond to each other at different frequencies. The greater the values, the stronger the correlation. Figures 5 and 6 compare the time series and MSCF between the acceleration measured from the reference accelerometers and smartphones.

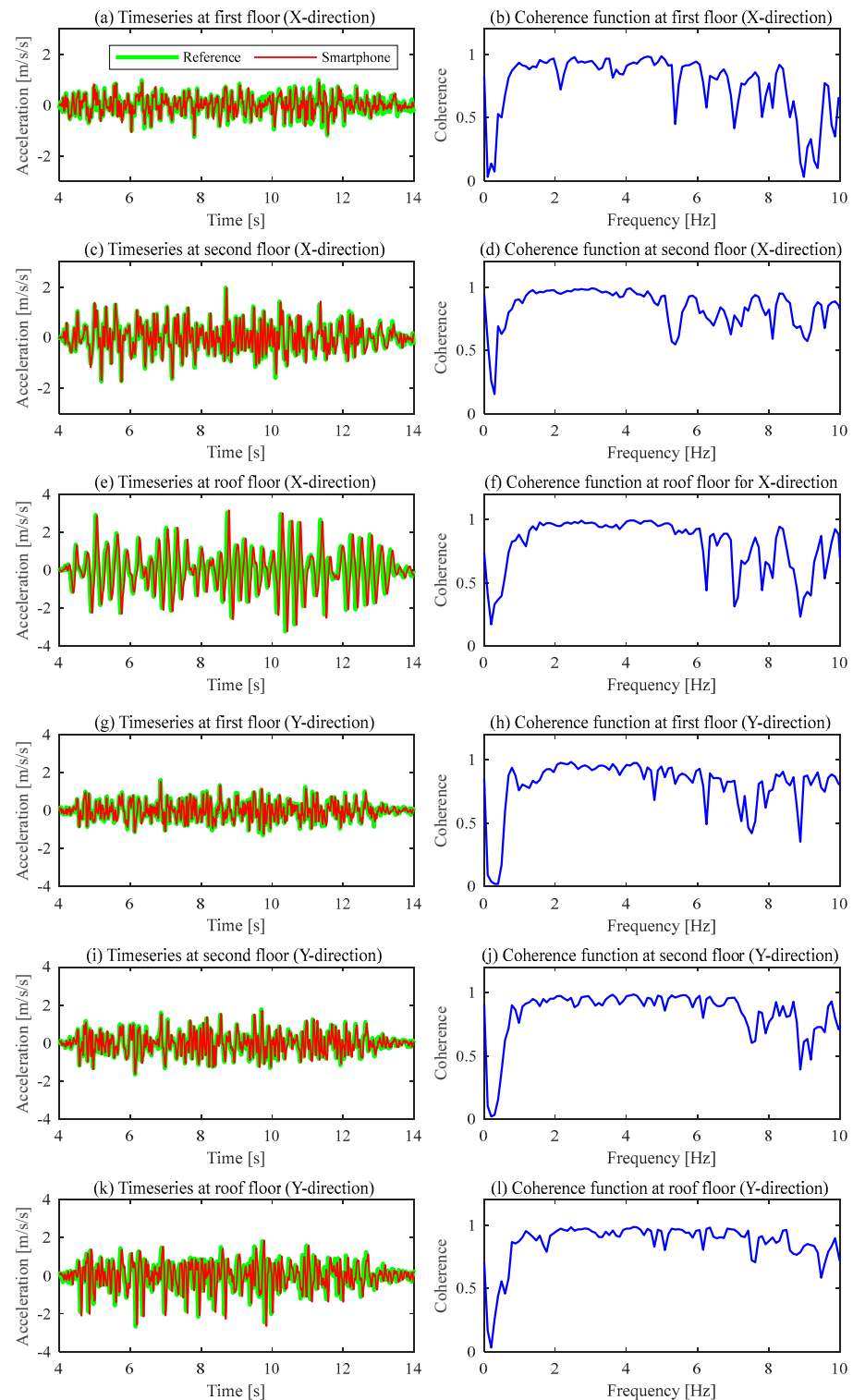


Figure 5. Comparison of time series between acceleration obtained from reference accelerometers and smartphones, and coherence for the X and Y directions in test 3.

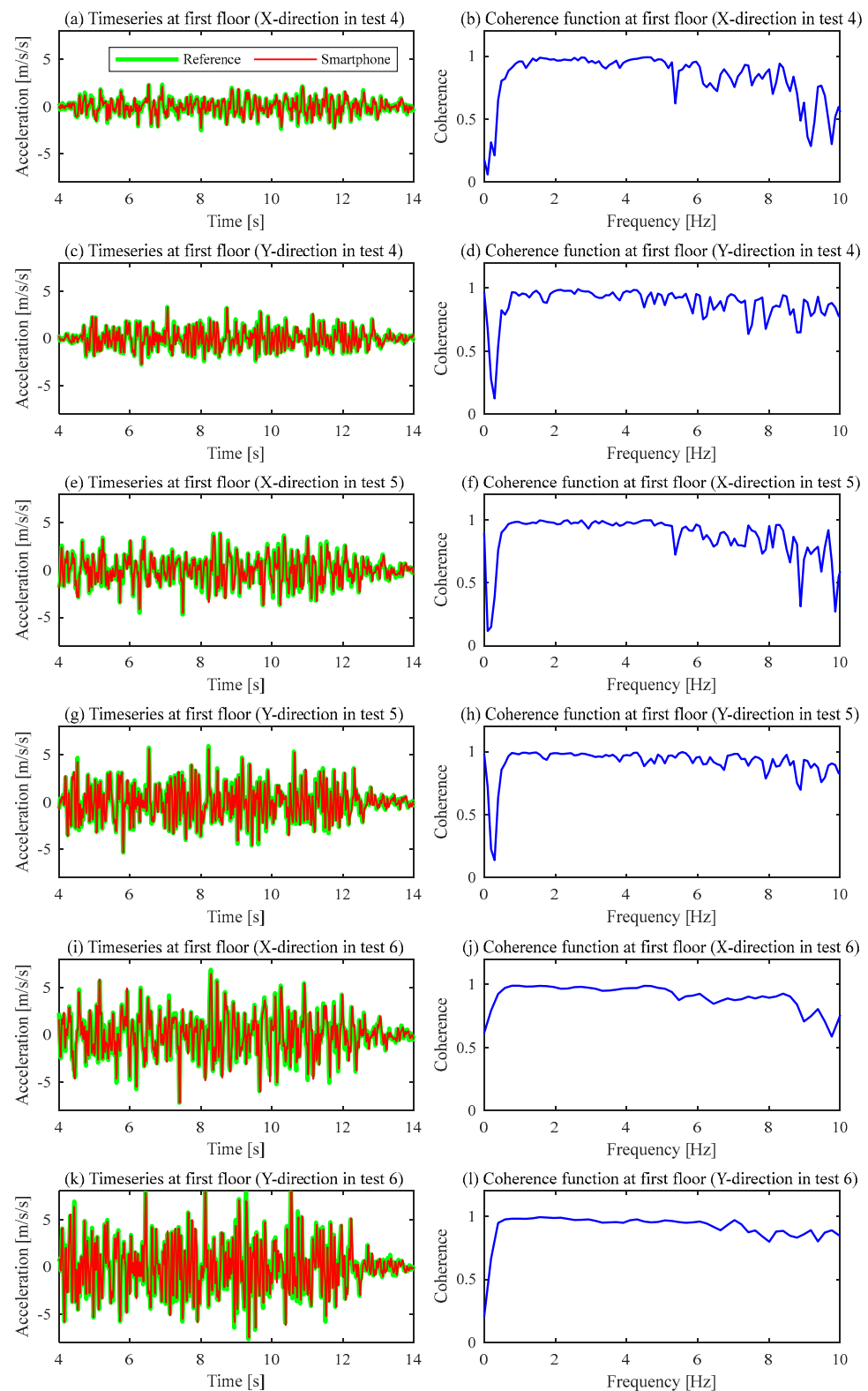


Figure 6. Comparison of time series between acceleration obtained from reference accelerometers and smartphones, and coherence for the X and Y directions in tests 4 to 6.

In Figure 5, the acceleration on each floor measured in test 3 was compared. The maximum accelerations measured with the reference accelerometers were 1.61 m/s^2 (Y direction) on the first floor, 1.97 cm/s^2 (X direction) on the second floor, and 3.22 cm/s^2 (X direction) on the third floor. On the other hand, the maximum accelerations measured

with the smartphones were 1.21 cm/s^2 (Y direction) on the first floor, 1.95 cm/s^2 (X direction) on the second floor, and 3.22 cm/s^2 (X direction) on the third floor. The ratio between the maximum acceleration values measured with the smartphones and reference accelerometers ranged from 95.8 to 99.9% in the X direction and from 95.8 to 99.9% in the Y direction. In other words, the maximum acceleration measured with iOS smartphones has an accuracy of 95% or higher. The RMSPE values ranged from 0.16 (X direction) to 0.19 (Y direction) on the first floor, from 0.22 (X direction) to 0.25 (Y direction) on the second floor, and from 0.57 (X direction) to 0.51 (Y direction) on the third floor. In other words, the RMSPE increased as the amplitude increased, but the accuracy can be considered to be high because the RMSPE is small. The MSCF in the X direction showed a tendency to decrease at 6 Hz or higher, but it can be considered that the two waveforms are in good agreement with each other because they are close to 1 and between 1 and 6 Hz. In particular, high agreement was observed in the Y direction on the third floor, where the amplitude was large.

In Figure 6, the acceleration on the first floor measured in tests 4 to 6 was compared. As in test 3 (Figure 5), high agreement was observed in the time series. The MSCF was also high in the Y direction. In test 6, in particular, it can be said that the accuracy is high, because the MSCF is close to 1 under 10 Hz. In tests 4 to 6, the ratio between the maximum acceleration values measured with the smartphones and reference accelerometers ranged from 92.6 to 100.1% in the X direction and from 91.0 to 98.9% in the Y direction, which are lower compared to test 3. The minimum and maximum RMSPE values were 0.23 (test 4) and 0.89 (test 6) in the X direction and 0.41 (test 4) and 1.18 (test 6) in the Y direction. In other words, as the amplitude increased, the RMSPE in the Y direction also increased. It is judged, however, that the smartphones used in this study can be employed for acceleration measurements because the RMSPE is small.

3.4. Displacement Estimation Accuracy

When a structure experiences harmonic motion, the relation $d(t) = \frac{a(t)}{-\omega^2}$ is widely used to determine the displacement, $d(t)$, from the acceleration, $a(t)$. Here, ω is the angular frequency. The same relation was also used in this study, and the displacement was estimated after converting the acceleration data measured with the smartphones into the frequency domain through FFT. These estimated values were compared with the displacement of each floor obtained from the experiment. The experimental displacements on the second and roof floors were the average values obtained by two wire displacement sensors installed on slabs on these floors. The displacement on the first floor was recorded using the shaking table control system. Figures 7 and 8 compare the total displacement in test 3 and in tests 4 and 5, respectively. In the figures, the displacements are compared only in the time period between 4 and 10 s, when the displacement amplitudes were relatively large. In test 3 (Figure 7), the ratio between the maximum displacements measured with the wire displacement sensors and smartphones ranged from 95.8 to 99.9% in the X direction and from 94.8 to 99.1% in the Y direction. The RMSPE values ranged from 0.16 (X direction) to 0.19 (Y direction) on the first floor, from 0.14 (X direction) to 0.16 (Y direction) on the second floor, and from 0.16 (X direction) to 0.17 (Y direction) on the third floor. In tests 4 to 6 where the amplitude was large (Figure 8), the ratio between the maximum displacement values measured with the wire displacement sensors and smartphones ranged from 92.6% (test 4) to 100.1% (test 6) in the X direction and from 91.0% (test 6) to 98.9% (test 4) in the Y direction. The accuracy showed a tendency to increase as the amplitude increased in the X direction; however, the same tendency was not observed in the Y direction. The minimum and maximum RMSPE values were 0.23 (test 4) and 0.89 (test 6) in the X direction, and 0.41 (test 4) and 1.18 (test 6) in the Y direction, which were the same as the acceleration RMSPE values. In other words, when the displacement is estimated using smartphones, an accuracy of 90% or higher can be obtained, even though the accuracy differs depending on the axial direction of the smartphone.

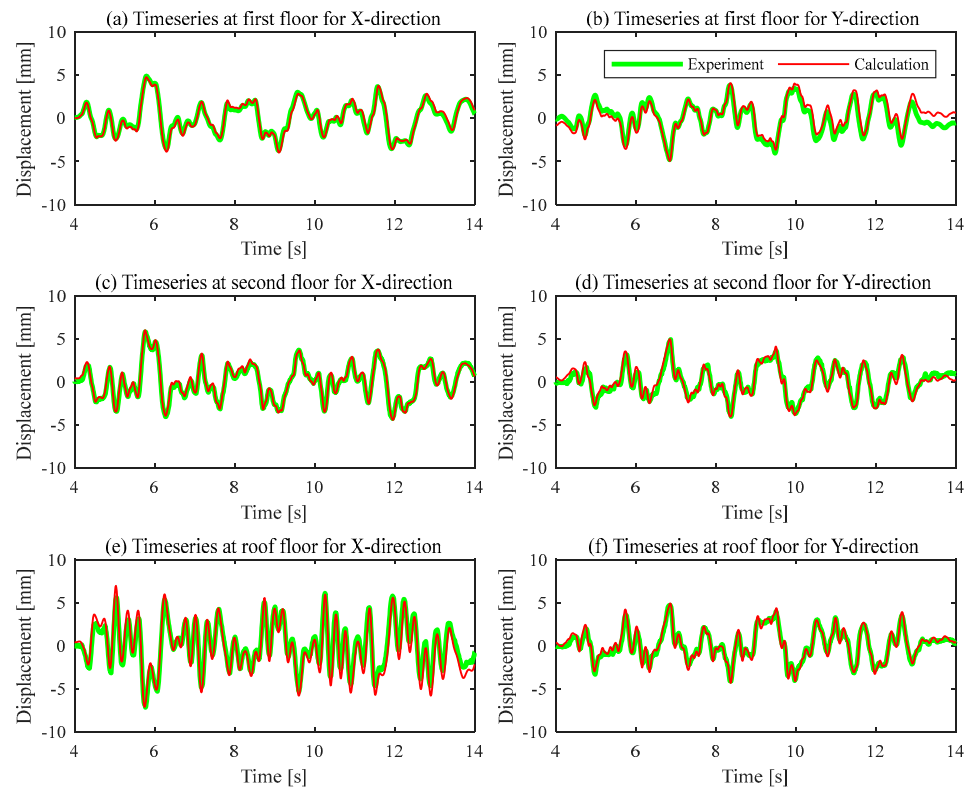


Figure 7. Comparison of displacements calculated by acceleration measured from reference accelerometers and smartphones along the X and Y directions in test 3.

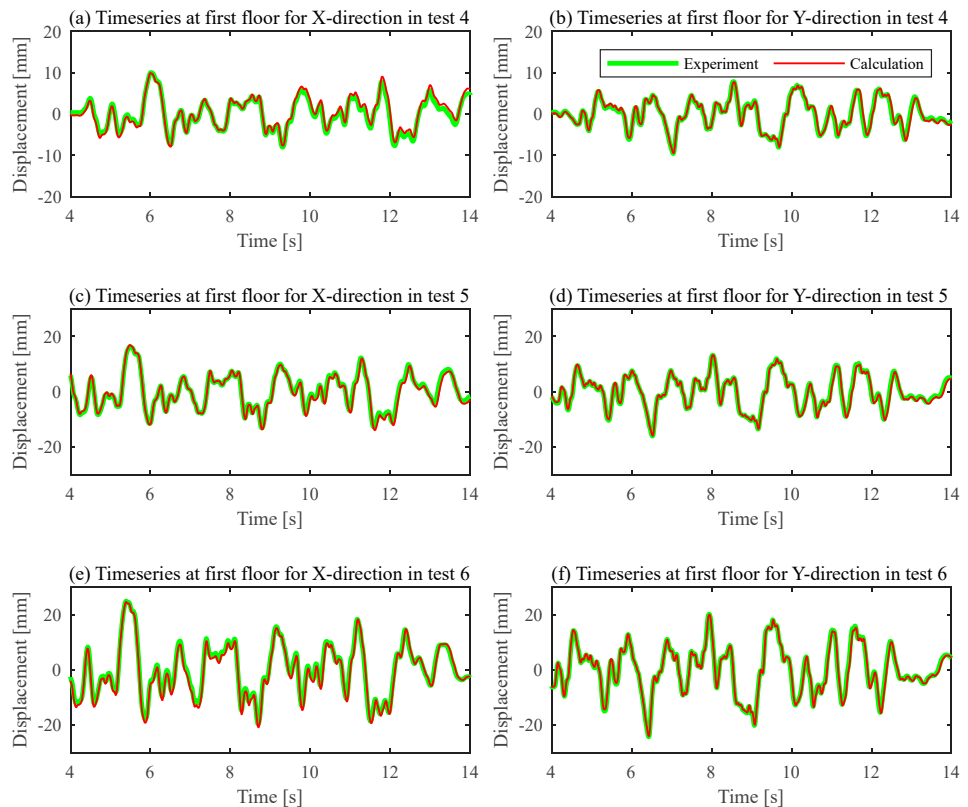


Figure 8. Comparison of displacements calculated using acceleration measured by reference accelerometers and smartphones along the X and Y directions in tests 4 to 6.

3.5. Estimation Accuracy of Interstory Drift Ratio (IDR)

When the safety of a building is evaluated after an earthquake, the interstory drift ratio (IDR) is one of the main evaluation indicators. Since the final purpose of this study is to examine the applicability of smartphones in building safety evaluation, this study also compared the IDR estimated from smartphone data with that calculated from the displacement sensors. Figure 9 compares the IDR values for test 3. The ratios between the maximum IDR obtained from the wire displacement sensors and that calculated from the smartphone data ranged from 114% (1 story) to 100% (2 story) in the X direction and from 104% (1 story) to 99% (2 story) in the Y direction. On the first floor in the X direction and the second floor in the Y direction with low IDRs, there is a difference between the IDR obtained from the displacement sensors and that obtained from the smartphone data. On the second floor in the X direction and the first floor in the Y direction, where the IDR was 0.1% or higher, however, that obtained from the smartphone data was similar to that obtained from the displacement sensors. In other words, it is concluded that the accuracy of the IDR estimated from the smartphone data is low when IDR is less than 0.1%, which is considered as the elastic range in building design; nevertheless, the IDR can be sufficiently estimated using smartphones when the IDR is 0.1% or higher.

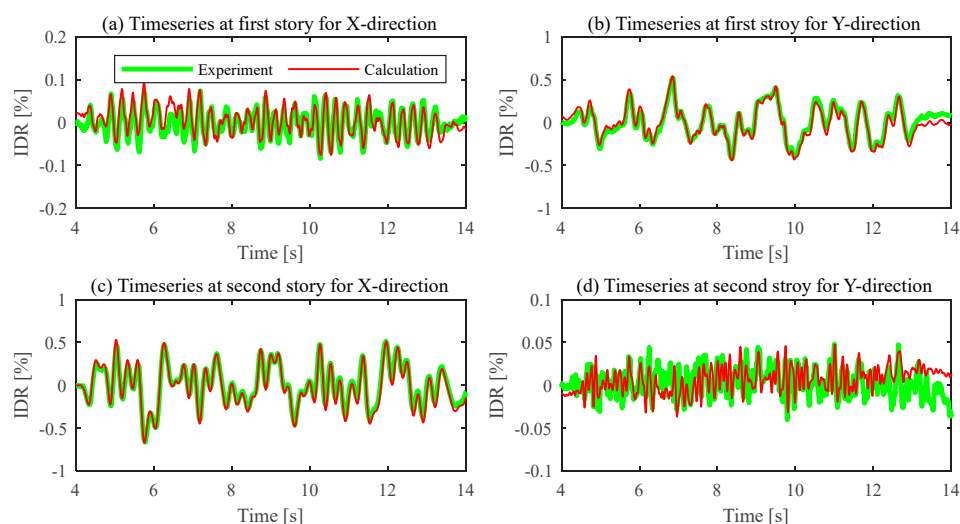


Figure 9. Comparison of interstory drift ratios (IDRs) estimated using accelerations measured by reference accelerometers and smartphones along the X and Y directions in test 3.

4. Conclusions

In this study, the applicability of smartphones to SHM, the prevalence of which is increasing worldwide, was verified by comparing the data measured using reference accelerometers and wire displacement sensors installed on the specimen through shaking table tests. For estimating the building deformation, which is related to building stability, the measurement performance for large deformation using smartphones was verified. A scale model of a masonry-filled RC frame building was used as the specimen, designed based on standard schematics for school buildings. The results of the shaking table test with smartphones can be summarized as follows.

1. During the shaking table test, some experimental data were lost due to issues with the power supply and the smartphone damage caused by impact; this indicates the need for mitigating measures in SHM use. In addition, there were time synchronization issues for each device when the Wi-Fi communication was incomplete, highlighting the need for continuous time synchronization or time synchronization post data collection. For using smartphones on the SHM in the future, an application, which enables time synchronization between smartphones installed in the same building, recording ambient vibration, and using low power, is necessary.

2. The natural period of the building evaluated using the smartphone coincided with that obtained from the reference accelerometer. This implies that smartphones can be used to measure the natural period of a building if the vibration occurs with the same magnitude as in the white noise excitation test.
3. The ratio between the maximum acceleration values measured with the smartphones and reference accelerometers ranged from 91.0 to 100.1%, and the MSCF ranged from 0.16 to 1.18. Hence, when the maximum acceleration is evaluated with a smartphone, an accuracy of 90% or higher can be expected.
4. The ratio between the displacement estimated from the acceleration data using smartphones and that obtained from the wire displacement sensors ranged from 91.0 to 100.1%, and the MSCF ranged from 0.14 to 0.86, confirming that the smartphone offered a displacement measurement accuracy of 90% or higher.
5. The ratio between the maximum IDR obtained from the wire displacement sensors and that calculated from the smartphone data ranged from 99% (two stories along the Y direction) to 114% (one story along the X direction). On the second floor in the X direction and the first floor in the Y direction, where the IDR was 0.1% or higher, the IDR obtained from the smartphone data was similar to that obtained from the displacement sensors. Thus, the IDR measurement accuracy using smartphones is low for IDRs less than 0.1%, which is considered as the elastic range in building design, but is sufficient when the IDR is 0.1% or higher.

Author Contributions: Conceptualization, J.-D.K.; experiment, J.-D.K., E.-R.B. and S.-H.P.; analysis, J.-D.K.; investigation, J.-D.K. and E.-R.B.; data curation, J.-D.K.; writing—original draft preparation, J.-D.K.; writing—review and editing, E.-R.B.; shaking table experimental supervision, E.-R.B.; phone experimental supervision, J.-D.K.; funding acquisition, J.-D.K. All authors have read and agreed to the published version of the manuscript.

Funding: This work was supported by Seoul Institute of Technology (SIT) (2021-AF-001 and 2022-AF-003).

Institutional Review Board Statement: Not applicable.

Informed Consent Statement: Not applicable.

Data Availability Statement: The data that support the findings of this study are available from the corresponding author, upon reasonable request.

Conflicts of Interest: The authors declare no conflict of interest.

References

1. Takahashi, R. The “SMAC” strong motion accelerograph and other latest instruments for measuring earthquakes and building vibrations. In Proceedings of the 1st World Conference on Earthquake Engineering, San Francisco, CA, USA, 12–15 June 1956; pp. 1–11.
2. Kanda, K.; Nakashima, M.; Suzuki, Y.; Ogasawara, S. “q-NAVI”: A case of market-based implementation of structural health monitoring in Japan. *Earthq. Spectra* **2021**, *37*, 160–179. [[CrossRef](#)]
3. Japan National Committee on Earthquake Engineering. Niigata Earthquake of 1964. In Proceedings of the Third World Conference on Earthquake Engineering, Auckland and Wellington, New Zealand, 22 January–1 February 1965; pp. 78–109.
4. Available online: <https://earthquake.usgs.gov/monitoring/nsmp/history/> (accessed on 12 March 2023).
5. Astorga, A.; Guéguen, P.; Ghimire, S.; Kashima, T. NDE1.0: A new database of earthquake data recordings from buildings for engineering applications. *Bull. Earthq. Eng.* **2020**, *18*, 1321–1344. [[CrossRef](#)]
6. Péquegnat, C.; Guéguen, P.; Hatzfeld, D.; Langlais, M. The French accelerometric network (RAP) and national data centre (RAP-NDC). *Seism. Res. Lett.* **2008**, *79*, 79–89. [[CrossRef](#)]
7. Dolce, M.; Nicoletti, M.; De Sortis, A.; Marchesini, S.; Spina, D.; Talanas, F. Osservatorio sismico delle strutture: The Italian structural seismic monitoring network. *Bull. Earthq. Eng.* **2017**, *15*, 621–641. [[CrossRef](#)]
8. Richardson, M. *Detection of Damage in Structures from Changes in Their Dynamic (Modal) Properties—A Survey (UCRL-15103)*; Structural Measurement Systems, Inc.: Santa Clara, CA, USA, 1979. [[CrossRef](#)]
9. Doebling, S.W.; Farrar, C.R.; Prime, M.B.; Shevitz, D.W. *Damage Identification and Health Monitoring of Structural and Mechanical Systems from Changes in Their Vibration Characteristics: A Literature Review*; Los Alamos National Laboratory report LA-13070-MS; Los Alamos National Laboratory: New Mexico, NM, USA, 1996.

10. Sivasuriyan, A.; Vijayan, D.S.; Górski, W.; Wodzyński, Ł.; Vaverková, M.D.; Koda, E. Practical implementation of structural health monitoring in multi-story buildings. *Buildings* **2021**, *11*, 263. [[CrossRef](#)]
11. Shokravi, H.; Shokravi, H.; Bakhary, N.; Rahimian Koloor, S.S.; Petru, M. Health monitoring of civil infrastructures by subspace system identification method: An overview. *Appl. Sci.* **2020**, *10*, 2786. [[CrossRef](#)]
12. Sohn, H.; Farrar, C.R.; Hemez, F.M.; Shunk, D.D.; Stinemates, D.W.; Nadler, B.R.; Czarnecki, J.J. *A Review of Structural Health Monitoring Literature: 1996–2001*; Los Alamos National Laboratory Report LA-UR-02-2095; Los Alamos National Laboratory: New Mexico, NM, USA, 2003.
13. Ko, J.M.; Ni, Y.Q. Technology developments in structural health monitoring of large-scale bridges. *Eng. Struct.* **2005**, *27*, 1715–1725. [[CrossRef](#)]
14. Farrar, C.R.; Worden, K. An introduction to structural health monitoring. *Philos. Trans. R. Soc. A* **2007**, *365*, 303–315. [[CrossRef](#)]
15. Kurka, P.R.G.; Cambraia, H.N. Application of a multivariable input–output subspace identification technique in structural analysis. *J. Sound Vib.* **2008**, *312*, 461–475. [[CrossRef](#)]
16. Li, H.N.; Ren, L.; Jia, Z.G.; Yi, T.H.; Li, D.S. State-of-the-art in structural health monitoring of large and complex civil infrastructures. *J. Civ. Struct. Health Monit.* **2016**, *6*, 3–16. [[CrossRef](#)]
17. Fan, W.; Qiao, P. Vibration-based damage identification methods: A review and comparative study. *Struct. Health Monit.* **2011**, *10*, 83–111. [[CrossRef](#)]
18. Artese, S.; Zinno, R. TLS for dynamic measurement of the elastic line of bridges. *Appl. Sci.* **2020**, *10*, 1182. [[CrossRef](#)]
19. Wu, B.; Wu, G.; Yang, C.; He, Y. Damage identification method for continuous girder bridges based on spatially-distributed long-gauge strain sensing under moving loads. *Mech. Syst. Signal Process.* **2018**, *104*, 415–435. [[CrossRef](#)]
20. Zhu, Y.; Ni, Y.Q.; Jin, H.; Inaudi, D.; Laory, I. A temperature-driven MPCA method for structural anomaly detection. *Eng. Struct.* **2019**, *190*, 447–458. [[CrossRef](#)]
21. Yu, Z.; Xia, H.; Goicolea, J.M.; Xia, C. Bridge damage identification from moving load induced deflection based on wavelet transform and Lipschitz exponent. *Int. J. Struct. Stab. Dyn.* **2016**, *16*, 1550003. [[CrossRef](#)]
22. Ozer, E.; Feng, M.Q. Structural reliability estimation with participatory sensing and mobile cyber-physical structural health monitoring systems. *Appl. Sci.* **2019**, *9*, 2840. [[CrossRef](#)]
23. Benz, H.; Buland, R.; Filson, J.; Frankel, A.; Shedlock, K. The advanced national seismic system. *Seism. Res. Lett.* **2001**, *72*, 70–75. [[CrossRef](#)]
24. Aoi, S.; Kunugi, T.; Fujiwara, H. Strong-motion seismograph network operated by NIED: K-NET and KiK-net. *J. Jpn. Assoc. Earthq. Eng.* **2004**, *4*, 65–74. [[CrossRef](#)]
25. Scislo, L. High activity earthquake swarm event monitoring and impact analysis on underground high energy physics research facilities. *Energies* **2022**, *15*, 3705. [[CrossRef](#)]
26. Scislo, L.; Guinchard, M. Source based measurements and monitoring of ground motion conditions during civil engineering works for high luminosity upgrade of the LHC. In Proceedings of the 26th International Congress on Sound and Vibration, Montreal, Canada, 7–11 July 2019.
27. Hsu, T.Y.; Yin, R.C.; Wu, Y.M. Evaluating post-earthquake building safety using economical MEMS seismometers. *Sensors* **2018**, *18*, 1437. [[CrossRef](#)]
28. Koide, E.; Fukuwa, N.; Masaki, K.; Hara, T.; Ohta, K.; Itoigawa, K. Development of low-cost seismograph for building response through internet. *J. Architect. Build. Sci. (AII)* **2006**, *23*, 453–458.
29. Albarbar, A.; Badri, A.; Sinha, J.K.; Starr, A. Performance evaluation of MEMS accelerometers. *Measurement* **2009**, *42*, 790–795. [[CrossRef](#)]
30. Cochran, E.S.; Lawrence, J.F.; Christensen, C.; Jakka, R.S. The quake-catcher network: Citizen science expanding seismic horizons. *Seismol. Res. Lett.* **2009**, *80*, 26–30. [[CrossRef](#)]
31. Bennett, V.; Abdoun, T.; Shantz, T.; Jang, D.; Thevanayagam, S. Design and characterization of a compact array of MEMS accelerometers for geotechnical instrumentation. *Smart Struct. Syst.* **2009**, *5*, 663–679. [[CrossRef](#)]
32. Lawrence, J.F.; Cochran, E.S.; Chung, A.; Kaiser, A.; Christensen, C.M.; Allen, R.; Baker, J.W.; Fry, B.; Heaton, T.; Kilb, D.; et al. Rapid earthquake characterization using MEMS accelerometers and volunteer hosts following the M 7.2 Darfield, New Zealand, earthquake. *Bull. Seismol. Soc. Am.* **2014**, *104*, 184–192. [[CrossRef](#)]
33. Milne, D.; Le Pen, L.; Watson, G.; Thompson, D.; Powrie, W.; Hayward, M.; Morley, S. Proving MEMS technologies for smarter railway infrastructure. *Procedia Eng.* **2016**, *143*, 1077–1084. [[CrossRef](#)]
34. Bedon, C.; Bergamo, E.; Izzi, M.; Noè, S. Prototyping and validation of MEMS accelerometers for structural health monitoring—The case study of the Pietratagliata cable-stayed bridge. *J. Sens. Actuator Netw.* **2018**, *7*, 30. [[CrossRef](#)]
35. Girolami, A.; Brunelli, D.; Benini, L. Low-cost and distributed health monitoring system for critical buildings. In Proceedings of the 2017 IEEE Workshop on Environmental, Energy, and Structural Monitoring Systems (EESMS), Milan, Italy, 24–25 July 2017.
36. Kong, Q.; Allen, R.M.; Schreier, L.; Kwon, Y.W. MyShake: A smartphone seismic network for earthquake early warning and beyond. *Sci. Adv.* **2016**, *2*, e1501055. [[CrossRef](#)]
37. Naito, S.; Azuma, H.; Senna, S.; Yoshizawa, M.; Nakamura, H.; Hao, K.X.; Fujiwara, H.; Hirayama, Y.; Yuki, N.; Yoshida, M. Development and testing of a mobile application for recording and analyzing seismic data. *J. Disaster Res.* **2013**, *8*, 990–1000. [[CrossRef](#)]

38. Shrestha, A.; Dang, J.; Wang, X. Development of a smart-device-based vibration-measurement system: Effectiveness examination and application cases to existing structure. *Struct. Control Health Monit.* **2018**, *25*, e2120. [[CrossRef](#)]
39. Jung, Y.S.; Yoon, S.W. The analysis in measurement performance MEMS sensor through the low-noise vibration measurement APP. *J. Korean Assoc. Spat. Struct.* **2017**, *17*, 93–100. [[CrossRef](#)]
40. Feng, M.; Fukuda, Y.; Mizuta, M.; Ozer, E. Citizen sensors for SHM: Use of accelerometer data from smartphones. *Sensors* **2015**, *15*, 2980–2998. [[CrossRef](#)] [[PubMed](#)]
41. Ozer, E.; Feng, M.Q. Synthesizing spatiotemporally sparse smartphone sensor data for bridge modal identification. *Smart Mater. Struct.* **2016**, *25*, 085007. [[CrossRef](#)]
42. Matarazzo, T.; Vazifeh, M.; Pakzad, S.; Santi, P.; Ratti, C. Smartphone data streams for bridge health monitoring. *Procedia Eng.* **2017**, *199*, 966–971. [[CrossRef](#)]
43. Guzman-Acevedo, G.M.; Vazquez-Becerra, G.E.; Millan-Almaraz, J.R.; Rodriguez-Lozoya, H.E.; Reyes-Salazar, A.; Gaxiola-Camacho, J.R.; Martinez-Felix, C.A. GPS, accelerometer, and smartphone fused smart sensor for SHM on real-scale bridges. *Adv. Civ. Eng.* **2019**, *2019*, 6429430. [[CrossRef](#)]
44. Shrestha, A.; Dang, J. Deep learning-based real-time auto classification of smartphone measured bridge vibration data. *Sensors* **2020**, *20*, 2710. [[CrossRef](#)]
45. Han, R.; Zhao, X. Shaking Table Tests and Validation of Multi-Modal Sensing and Damage Detection Using Smartphones. *Buildings* **2021**, *11*, 477. [[CrossRef](#)]
46. Roman-Stork, H.L.; Subrahmanyam, B.; Murty, V.S.N. Quasi-biweekly oscillations in the Bay of Bengal in observations and model simulations. *Deep Sea Res. Part II Top. Stud. Oceanogr.* **2019**, *168*, 104609. [[CrossRef](#)]
47. Nadarajah, S. Comments on “Approximation of statistical distribution of magnitude squared coherence estimated with segment overlapping”. *Signal Process.* **2007**, *87*, 2834–2836. [[CrossRef](#)]
48. Pan, G.; Li, S.; Zhu, Y. A time-frequency correlation analysis method of time series decomposition derived from synchrosqueezed S transform. *Appl. Sci.* **2019**, *9*, 777. [[CrossRef](#)]

Disclaimer/Publisher’s Note: The statements, opinions and data contained in all publications are solely those of the individual author(s) and contributor(s) and not of MDPI and/or the editor(s). MDPI and/or the editor(s) disclaim responsibility for any injury to people or property resulting from any ideas, methods, instructions or products referred to in the content.